Available online at www.sciencedirect.com

ScienceDirect

Physics Procedia 10 (2010) 189–196

Physics Procedia

www.elsevier.com/locate/procedia

3rd International Symposium on Shape Memory Materials for Smart Systems

A Bistable Magnetically Enhanced Shape Memory Microactuator With High Blocking Forces

J. Barth* and M. Kohl

Karlsruhe Institute of Technology (KIT), IMT, Hermann-von-Helmholtz-Platz 1, 76344 Eggenstein-Leopoldshafen, Germany

Abstract

A novel approach of combining nonmagnetic shape memory alloy (SMA) microactuators with electroplated magnetic layers (ML) is presented, which enables the use of two intrinsic actuation principles in a single SMA-ML component allowing considerable gain in functionality. In the present work, we demonstrate local electroplating of Ni-81.75at.%Fe discs onto the surface of Ti-49at.%Ni microbridge structures. Antagonistic SMA-ML microactuators are fabricated by mechanically coupling two SMA-ML microbridges in their center by a spacer and prestraining them with respect to each other. The SMA-ML microactuators show bistable performance in the presence of an inhomogenous magnetic field generated by permanent magnets near the magnetic discs. Compared to antagonistic SMA microactuators fabricated without electroplated discs, a considerable improvement of mechanical performance is achieved. Magnetically enhanced SMA-ML microactuators of 7x7x4 mm^3 overall size show a blocking force and bistable stroke of about 33 mN and 84 µm, respectively, while corresponding conventional SMA microactuators show no blocking force and a considerably smaller bistable stroke of 15 µm.

Keywords: bistable switch; microactuation; shape memory alloys; permalloy; electroplating

1. Introduction

Shape memory alloys (SMAs) are promising smart materials to realize actuation in small dimensions due to their high energy density and favorable down-scaling behavior [1]. A number of SMA microactuators have been developed up to now that meet the requirements in various microsystems applications [2-4]. Ti-Ni microbridge actuators have been used, e.g., for microvalve applications displaying work densities larger than 10 J/mm^3 [1].

Because of the thermal SMA effect, major drawbacks are the relatively high power consumption and the poor dynamics compared to other actuation principles like electrostatic or the inverse piezoelectric effect [1]. Both can be improved by miniaturization and combining shape recovery forces with the magneto-static forces of a soft-magnetic structure in the gradient field of a permanent magnet. This can be realized, e.g., by using ferromagnetic shape memory alloys (FSMAs) that has first been demonstrated for a FSMA microscanner operating in off-resonance

* Corresponding author. Tel.: +49 7247 82 2746; fax: +49 7247 82 4331.
E-mail address: johannes.barth@kit.edu

1875-3892
doi:10.1016/j.phpro.2010.11.097

mode at frequencies well above 100 Hz [4]. Here, we propose an alternative approach of combining conventional nonmagnetic SMAs with electroplated magnetic layers (ML). In this way, it is possible to make use of the well-established performance, e.g., of Ti-Ni and, at the same time, introduce additional magnetic functionality. The control of additional magneto-static forces may, for instance, enhance the performance of previous nonmagnetic SMA actuators or allow the development of novel combinations of magnetic and shape memory mechanisms, thus, opening up new applications.

Bistable actuation is important for applications with particular demands on the balance between low power consumption and high blocking forces. Examples are in mobile applications, where energy is lean and two defined switching positions have to be maintained against external forces. Compared to other bistable principles, e.g. electromagnetic [5,6] or pneumatic [7], bistable SMA-ML actuators may offer large switching and blocking forces based on relatively simple designs suitable for further miniaturization [8,9].

In the following, the material properties of the Ti-Ni foils and the electroplated Ni-Fe layers are introduced. Subsequent sections present the electro-thermo-mechanical performance of mechanically coupled SMA microbridges and the magneto-static attraction between different soft- and hard-magnetic structures. Finally, fabrication aspects and performance characteristics of antagonisitic SMA and SMA-ML microactuators are discussed.

2. SMA Material Properties

The used SMA is a cold-rolled Ti-49at.%Ni foil of 20 µm thickness. Fig. 1 shows a typical electrical resistance characteristic in the temperature regime of phase transformation. Above room temperature the material shows a R-phase transformation, which is characterized by a resistance increase upon cooling, starting at R_s = 325 K and ending at R_f = 312 K. Typically, the R-phase transformation exhibits a narrow hysteresis of a few Kelvin [10]. Upon further cooling, the martensitic transformation is observed showing a sharp drop at about 280 K. The martensite finish temperature is reached at about 230 K. In this investigation, we keep above room temperature. Therefore, upon thermal actuation by electrical heating, only R-phase transformation occurs. From an "engineer´s" perspective, the properties of the R-phase transformation are advantageous with respect to hysteresis, dynamics and fatigue resistance.

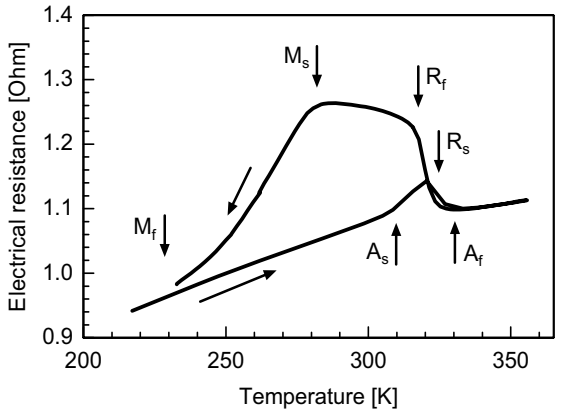

Fig. 1: Electrical resistance characteristic of the 20 µm thick cold-rolled Ti-Ni foil. The phase transformation temperatures are indicated by arrows.

3. Properties of Electroplated Ni-Fe on Ti-Ni

Electroplating is predestined for depositing of thick metal layers in micro engineering [11]. Compared to the methods of physical vapor deposition (PVD), like sputtering or evaporation, it has advantages of higher deposition

rates, lower mechanical stress and better material composition homogeneity [12]. Nevertheless, the starting surface and thus the interaction layer between the receptor and the plated material is a critical issue.

The Ti-Ni foil forms a native oxide on the surface with an average thickness of 1.5 µm. The oxide is first removed to avoid a strong undercut during structuring the Ti-Ni microbridges by wet-chemical etching. Subsequently, a 100 nm Au layer is deposited by magnetron sputtering to avoid re-oxidation. In addition, the Au layer is used as a mask in the subsequent wet-chemical etching process. Later on, the Au layer is removed to facilitate electroplating on an oxide-free Ti-Ni surface. The Ni-Fe electroplating is performed in a sulfate electrolyte bath at 51°C with $NiSO_4$, $Fe(II)SO_4$, boracic acid and saccharin. Ni is used as the anode material. The current-density is set to 0.6 A/dm^2. With this configuration, the deposition rates are up to 6 µm/h.

The properties of the Ni-Fe layer are investigated by energy dispersive X-ray (EDX) spectroscopy and alternating gradient magnetometer (AGM) measurements and (see Figs. 2 a and b, respectively). The EDX measurement (Fig. 2a) shows a Ni to Fe ratio of 81.7 to 18.3. Thus, a good saturation flux density is expected. The AGM measurements (Fig. 2b) confirm this result showing saturation flux densities B_S between 0.98 and 1.05 T. The Ni-Fe layer shows a very narrow hysteresis with a permeability μ_r between 70000 and 100000 and a remanence field B_R smaller than 0.05 T.

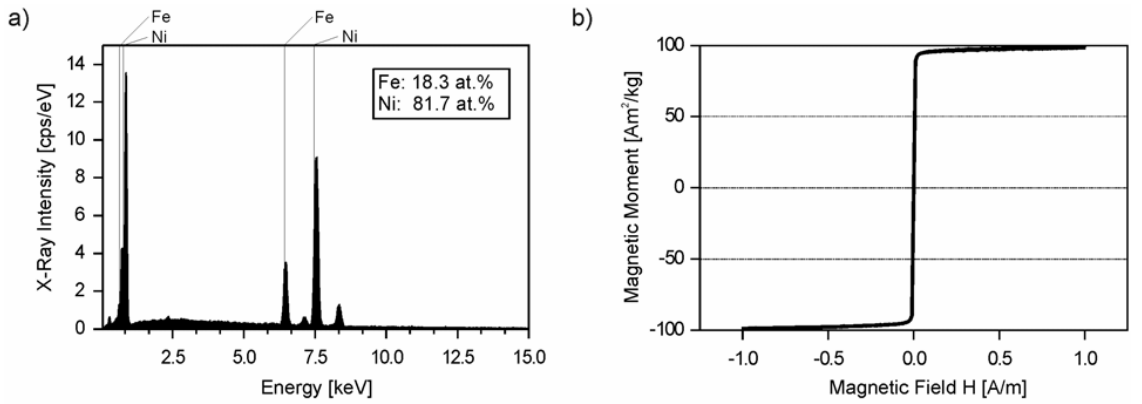

Fig.2: Material properties of electroplated Ni-Fe on a Ti-Ni substrate. a) Magnetic moment versus the applied magnetic field measured by an AGM b) X-ray spectrum showing typical spectral lines of Ni and Fe as indicated.

The Ni-Fe-layers adhere on the Ti-Ni foils very well even though no additional adhesion layers are used. Standard shear tests with a maximum force of 10 N show no destructive effect on the adhesion of Ni-Fe discs having a diameter of 800 µm. This can be understood by investigating the surface texture of the Ti-Ni layer by an atomic force microscope (AFM) in tapping mode. Fig. 3 shows typical results of the Ti-Ni surface before and after oxide etching as well as a magnification of a characteristic spot. The arithmetic average of the surface roughness Ra decreases from 128 to 97 nm after the oxide etching. In addition, large cavities with depth up to 700 nm are observed. Due to these cavities, the total surface area increases dramatically and the electroplated layer can interlock with the surface of the Ti-Ni substrate.

4. SMA Microbridge Structures

SMA microbridges are designed as basic components to perform out-of-plane actuation. As sketched in Fig. 4, a single microbridge consists of four freely suspended beams in a 90 degree arrangement. Each beam has an effective length, width and thickness of 1.5, 0.1 and 0.02 mm, respectively. All beams join at a center disc that is used as a support for the soft magnetic layer to be electroplated.

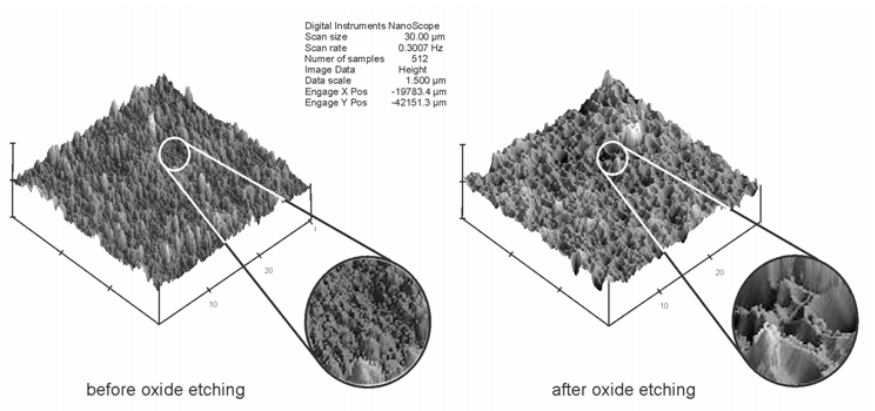

Fig.3: AFM-measurements of the TiNi surface before (left side) and after the removal of the oxide layer (right side).

The force-deflection characteristic of the microbridges has been investigated by a micro hook attached to a load-cell. The hook is fixed below the center of the bridge mounted on a linear stage. By driving the linear stage relatively to the hook the corresponding forces are determined. Fig. 4 shows a typical force-deflection curve of a single Ti-Ni microbridge at room temperature and in heated condition at $T>Af$. In both cases, the force increases non-linearly with increasing deflection. At room temperature, a maximum force of 50 mN is reached for an out-of-plane deflection of 200 µm. This force increases considerably upon heating the microactuator above the Af-temperature. The solid line represents a simulated force-deflection curve based on an elastic bridge model that assumes a simplified geometry with fixed end points and a point load in the center [1]. The stress and strain are assumed to be homogeneous. A deflection of about 160 µm corresponds to a strain of about 0.3 %, which is considered to be the maximum allowable strain in austenitic (A-) phase. The deflection in the R-phase state is limited by the transformation strain of about 0.8 % that corresponds to a maximum allowable out-of-plane deflection of 250 µm at room temperature.

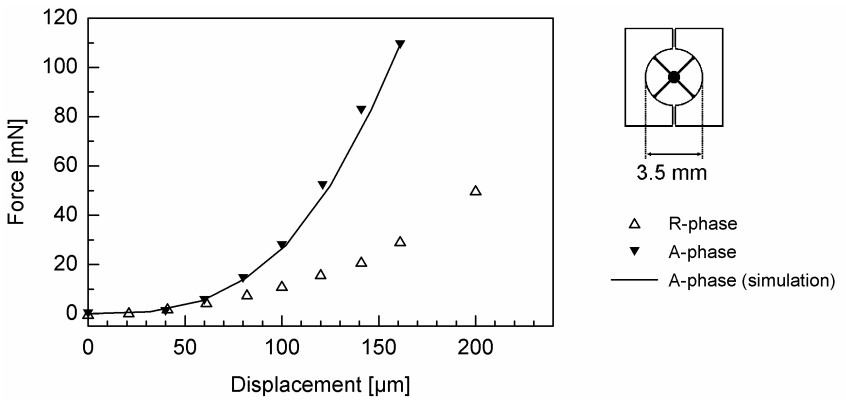

Fig. 4: Force-deflection characteristics of a single SMA microbridge in A- and R-phase. The inset shows a schematic of the SMA microbridge in top view.

An antagonistic SMA microactuator is designed by mechanically coupling the center of two SMA microbridges by a spacer and predeflecting them with respect to each other in out-of-plane direction as sketched in Fig. 5. In this case, the total predeflection d_{pre} is given by the difference of the spacer and the substrate thickness $h_{sp} - h_{sub}$ (Fig.

5a). By heating microbridge m1 with an electrical current (Fig. 5b), a transformation from R- to A-phase occurs. The increasing reset force drives the antagonistic SMA microactuator to its first point of force equilibrium E1, which is characterized by the equilibrium of the force of m1 being in A-phase and m2 being in R-phase condition: $F_{A1}(x_{E1})=F_{R2}(x_{E1})$. The second point of force equilibrium E2 (Fig. 5 c) is reached by selectively heating m2. Due to symmetry, the condition holds: $|x_{E2}| = |x_{E1}|$. The corresponding actuator displacement x is described by the motion of the spacer midpoint. Hence, the out-of-plane deflection of SMA microbridges m1 and m2 is $|d_{pre}/2 - x|$ and $|d_{pre}/2 + x|$, respectively.

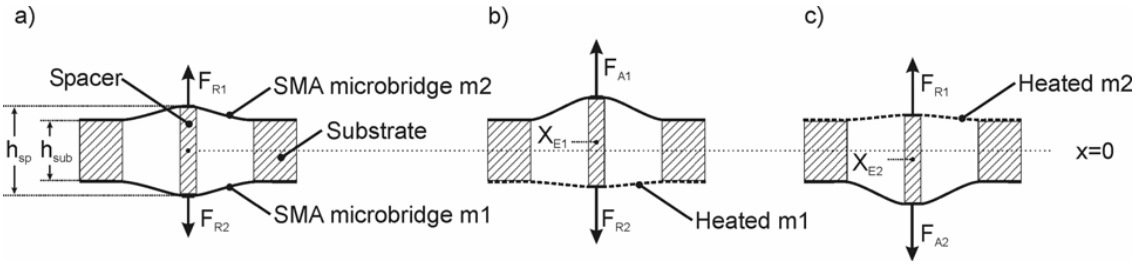

Fig. 5: Schematic cross section of an antagonistic SMA microactuator consiting of two mechanically coupled SMA microbridges in initial position (a), with heated microbridge m1 (b) and m2 (c).

It is obvious, that the end positions x_{E1} and x_{E2} can no longer be maintained after switching the heating power off. However, the microbridges can be kept in place by introducing additional magneto-static forces in the end positions. Useful extra forces are in the range between the minimum required extra force ΔF_{min} to maintain the equilibrium positions mi (i=1,2) in the power-off state (F_{Ai}-F_{Ri}) and the maximum extra force ΔF_{max}, which is an upper limit to enable switching by the SMA microbridges between the end positions. Any extra force above ΔF_{min} will provide an additional blocking force to be overcome in order to allow for switching. The forces ΔF_{min}, ΔF_{max} and actuation stroke s depend on the predeflection d_{pre} and can thus be determined from the force-deflection characteristics shown in Fig. 4. Typical results are listed in Table 1 for predeflections between 240 and 360 µm.

Table 1: Calculated actuation stroke s, minimum and maximum retention forces ΔF_{min} and ΔF_{max} depending on the total predeflection d_{pre}.

d_{pre} [µm]	s [µm]	ΔF_{min} [mN]	ΔF_{max} [mN]
240	53.3	15.7	78.9
280	67.0	23.7	128.6
300	74.1	28.5	159.8
320	81.3	33.7	195.6
360	96.2	45.8	282.4

5. Magnetic Layer Structures

A parameter study based on finite element (FE) simulation using FEMM [13] has been accomplished to determine the optimum geometries of the magnetic structures. In order to allow for easy fabrication, disc-shaped soft-magnetic and cylindrical-shaped hard-magnetic structures are considered. The magnetic properties of the plated soft-magnetic Ni-Fe are taken from the data in Fig. 2. Molded Nd-Fe-B hard magnets have been obtained from a commercial source showing a coercivity of 113.8E-4 A/m and an isotropic relative permeability of 1.049.

Fig. 6 gives an overview of simulated force-displacement characteristics obtained for different combinations of diameters and thicknesses of hard-magnetic cylinders and soft-magnetic discs assuming a displacement range of

± 35 µm. The inset of Fig. 6 shows the arrangement of the permanent magnets, the nonmagnetic spacer and the soft-magnetic discs for the simulation model. After each evaluation step, the spacer and the soft-magnetic discs are displaced in *x*-direction as highlighted, until the gap between the magnet and the upper soft-magnetic disc is 1 µm.

The simulations (1-3) show an increase of the gradient and the maximum magnetic force with decreasing diameter ratio $Ø_M/Ø_D$. Subsequent optimization [14] of the diameter ratio shows an optimum at $Ø_M/Ø_D$= 0.94. Obviously, small magnet diameters and correspondingly small diameter ratios are less favorable due to the limited field density. On the other hand, large magnet diameters are less favorable as well, because the soft-magnetic disc only senses the part of the magnetic field with low gradient. Additionally, an increase of the soft-magnetic disc thickness (3-4) leads to an increase of the gradient and the maximum magnetic force as well. Due to limitations of the electroplating process, the maximum thickness is set to 200 µm.

Best results are found for diameter/thickness of Nd-Fe-B cylinders and Ni-Fe discs of 750 µm/1000 µm and 800 µm/200 µm, respectively. In this case, the minimum required magnetic extra force ΔF_{min} of 28.5 mN for a predeflection d_{pre} of 300 µm is reached for relatively small displacements of |x| = 15 µm. In the end positions of |x| = 35 µm, the magnetic extra force exceeds ΔF_{min} by 60 mN.

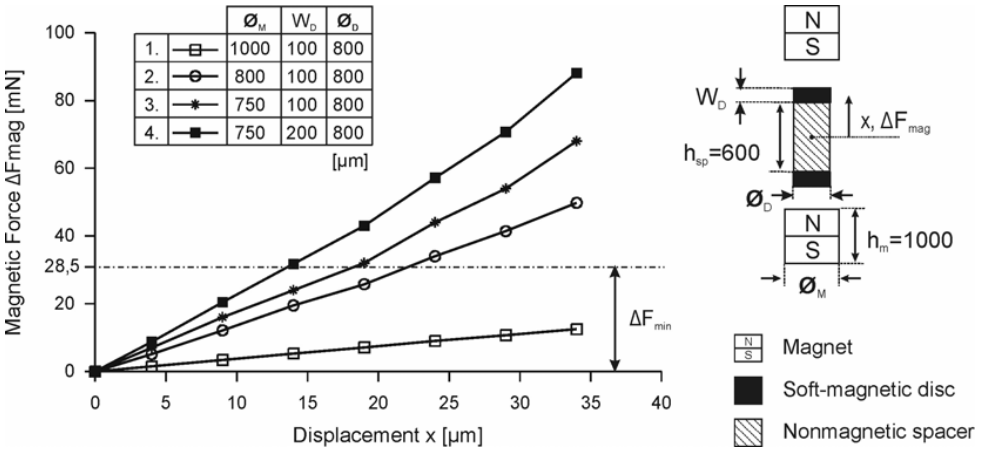

Fig. 6: Simulated resulting magnetic attraction force as a function of the displacement x. The inset shows schematically the configuration of the hard- and soft-magnetic structures for the simulation model.

6. Magnetically Enhanced SMA Microactuator

Demonstrators of SMA-ML microactuators are fabricated consisting of two antagonistic Ti-Ni microbridges with electroplated Ni-Fe discs at their center. The microbridges are fabricated on a support wafer by photolithography and wet chemical etching followed by a thick-film process for masking and the electroplating of the Ni-Fe disc. The 3D integration of the coupled antagonistic pair into the polymer-housing is accomplished by a two-step transfer bonding process [14]. The overall dimensions including the housing are 7x7x4 mm^3.

The performance of a SMA-ML microactuator is investigated by an optical video microscope to measure the stroke and by a micro load cell with a mounted magnet to measure the maximum blocking force. Fig. 7 shows the typical heating power-dependent displacement characteristics of a SMA-ML microactuator without (I.) and with permanent magnets (II.) for a pre-deflection of 300 µm in each case. The schematics illustrate the corresponding configuration of the microactuators in cross section. Successive heating and cooling of both SMA microbridges is required to pass through a complete actuation cycle. In the case of the SMA-ML microactuator (I.), the maximum stroke is 69 µm that agrees well with the estimated value of 74.1 µm (Table 1). By switching the heating power off after reaching the end position (a), elastic forces drive the system partially backwards towards an intermediate position (b) as long as magnetic forces are absent. In this case, only a quasi-bistable behavior with a stroke of about

15 µm occurs. In the presence of the inhomogeneous magnetic fields of two permanent magnets (II.), the SMA-ML microactuator shows a fully bistable behavior. Due to the magnetic extra forces the maximum stroke at P_{el} = 0 W can be tuned to s = 84 µm. Switching of the bistable microactuator occurs between 20 and 25 mW. The two switching states are shown as photographs in Fig. 7.

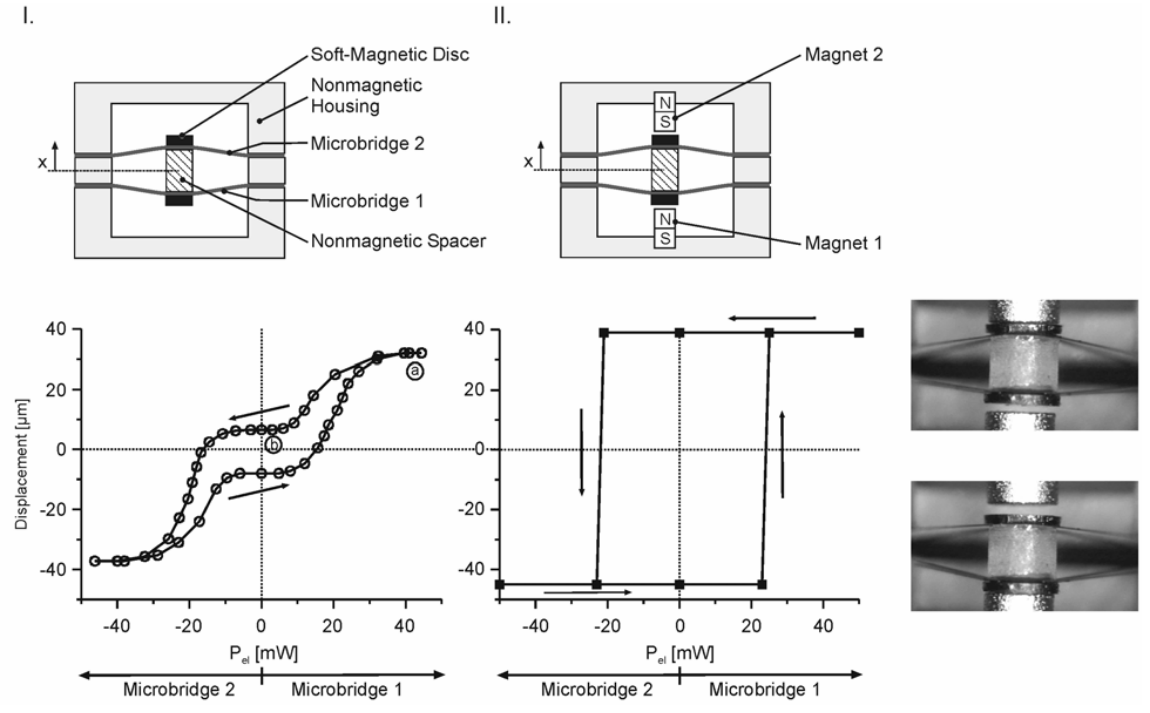

Fig.7: Full actuation cycle of the SMA-ML microactuator without (I.) and with external magnetic field of two Nd-Fe-B magnets (II.).The two switching states of the demonstrator are shown as photographs.

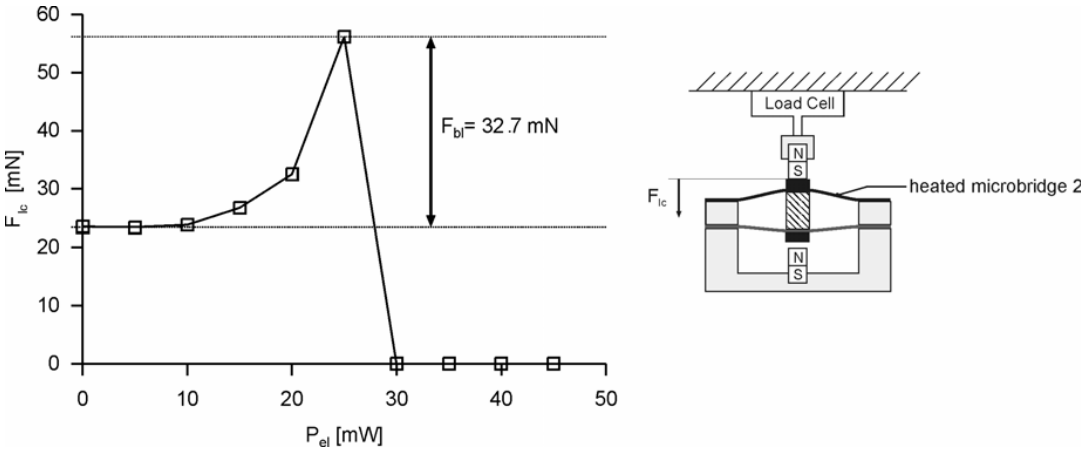

Fig.8: Heating power dependent force of the SMA-ML microactuator (II.) and resulting blocking force F_{bl}. The inset shows the corresponding measurement setup with magnet 2, mounted to a load cell.

To determine the blocking force of the SMA-ML microactuator (II.), magnet 2 is fixed to a load cell (see inset of Fig.8) and the measured force of the load cell F_{lc} is plotted against the electrical power of microbridge 2 (Fig. 8). The force F_{lc} = 23.3 mN at P_{el} = 0 corresponds to the calculated force ΔF_{min} = 28.5 mN and increases with subsequently increasing the electrical power of microbridge 2 until the Ni-Fe disc releases from the magnet. The difference of these two values equates to the maximum possible blocking force of the SMA-ML microactuator with ΔF_{bl}= 32.7 mN.

7. Conclusion And Outlook

We demonstrate the combined use of the two intrinsic actuation principles of shape recovery and magneto-static attraction in a novel SMA-ML microactuator consisting of magnetic layers on SMA microstructures. The present investigation focuses on Ni-Fe discs that are electroplated directly onto the surface of Ti-Ni microbridge structures after oxide removal. Two SMA-ML microbridge structures are mechanically coupled to perform antagonistic actuation in out-of-plane direction. In the presence of an inhomogeneous magnetic field, this SMA-ML microactuator shows bistable performance. In particular, a large blocking force and bistable stroke of about 33 mN and 84 µm, respectively, are achieved due to magnetic enhancement.

Besides the performance enhancement of SMA actuation by ML actuation reported here, various other functionalities may be realized by combining SMA and ML structures, e.g., SMA actuation and magnetic sensing or SMA sensing and magneto-static actuation. Thus, the presented technology approach enables the development of novel SMA-ML actuator-sensor systems and leads to new microsystems applications.

The achieved specifications of the bistable SMA-ML microactuator meets current requirements, e.g., for microrelais, micro optical switches and microvalves. Compared to conventional electromagnetic bistable actuators, no complex three-dimensional structures like coils are required.

References

[1] Kohl M, 2004 Shape memory microactuators *Springer-Verlag, Heidelberg.*
[2] Kohl M, Just E, Pfleging W and Miyazaki S, 2000 SMA microgripper with integrated antagonism *Sensors and Actuators* **A83** 208-213
[3] Kohl M, Dittmann D, Quandt E and Winzek B, 2000 Thin film shape memory microvalves with adjustable operation temperature *Sensors and Actuators* **A83** 214-219
[4] Kohl M, Brugger D, Ohtsuka M and Takagi T, 2004 A novel actuation mechanism on the basis of ferromagnetic SMA thin films *Sensors and Actuators* **114** 445-450
[5] Ren H and Gerhard E 1997, Design and fabrication of a current-pulse-excited bistable magnetic micro-actuator *Sensors and Actuators* **A58** 259-264
[6] Capanu M, Boyd J G and Hesketh P J, 2000 Design, fabrication and testing of a bistable electro-magnetically actuated microvalve *J. of microelectro-mechanical systems* **Vol. 9** 181-189
[7] Schomburg W K and Goll C, 1998 Design optimization of bistable microdiaphragm valves *Sensors and Actuators* **A 64** 259-264
[8] Barth J, Grund T, Krevet B and Kohl M, 2008 A Magnetic force-enhanced bistable shape memory microactuator *Proc. Actuator* **08** 386-389
[9] Barth J, Krevet B and Kohl M, 2009 A bistable SMA microactuator with large work output *Transducers 2009* 41-44
[10] Miyzaki S and Otsuka K, 1986 Deformation and transition behaviour associated with the R-phase in Ti-Ni alloys *Metall. Trans. A* **17A** 53-63
[11] Nosang V. Myung and D.-Y. Park, 2003 Development of electroplated magnetic materials for MEMS *Journal of Magnetism and Magnetic Materials* **265** 189-198
[12] Yong-hua Zhang, Gui-fu Ding, Yu-li Cai, Hong Wang and Bingchu Cai, 2008 Electroplating of low stress permalloy *Materials Characterization* **57** 121-126
[13] http://www.femm.info/wiki/HomePage
[14] J. Barth, B. Krevet and M. Kohl, 2010 A bistable shape memory microswitch, *Smart Mater. Struct.*, to be published.